Journal of Power Sources 272 (2014) 378–385

Contents lists available at ScienceDirect

Journal of Power Sources

journal homepage: www.elsevier.com/locate/jpowsour

Measurement of in-plane thermal conductivity and heat capacity of separator in Li-ion cells using a transient DC heating method

V. Vishwakarma, A. Jain*

Mechanical and Aerospace Engineering Department, University of Texas at Arlington, Arlington, TX, USA

HIGHLIGHTS

- Presents measurement of in-plane thermal conductivity and heat capacity of separator.
- Experimental data are in excellent agreement with analytical model.
- Measurements indicate very low thermal conductivity of the separator.
- Measurements indicate weak temperature dependence of thermal properties.
- Measurements presented here may facilitate high performance and safety.

ARTICLE INFO

Article history:
Received 17 May 2014
Received in revised form
26 July 2014
Accepted 16 August 2014
Available online 25 August 2014

Keywords:
Lithium-ion cells
Separator
Thermal conductivity
Heat capacity
Battery safety
Flexible substrates

ABSTRACT

The separator is a critical, multi-functional component of a Li-ion cell that plays a key role in performance and safety during energy conversion and storage processes. Heat flow through the separator is important for minimizing cell temperature and avoiding thermal runaway. Despite the critical nature of thermal conduction through the separator, very little research has been reported on understanding and measuring the thermal conductivity and heat capacity of the separator. This paper presents first-ever measurements of thermal conductivity and heat capacity of the separator material. These measurements are based on thermal response to an imposed DC heating within a time period during which an assumption of a thermally semi-infinite domain is valid. Experimental data are in excellent agreement with the analytical model. Comparison between the two results in measurement of the in-plane thermal conductivity and heat capacity of the separator. Results indicate very low thermal conductivity of the separator. Measurements at an elevated temperature indicate that thermal conductivity and heat capacity do not change much with increasing temperature. Experimental measurements of previously unavailable thermal properties reported here may facilitate a better fundamental understanding of thermal transport in a Li-ion cell, and enhanced safety due to more accurate thermal prediction.

1. Introduction

Thin flexible substrates are frequently used in engineering applications such as flexible electronics [1,2], separators for Li-ion cells [3–5], organic semiconductors [6], flexible displays [7–9], etc. Compared to a thick rigid substrate, a flexible substrate offers reduced weight, increased design flexibility, bendability, etc. [10]. In addition, thin substrates also often provide valuable functionality, such as controlled ionic conductance through thin separators in Li-ion cells [3]. The thin, flexible nature of the separator in a Li-ion cell also makes it possible to roll the electrode-separator assembly and compactly package it inside a high energy density cell [3]. Fig. 1 shows an image of the electrode-separator roll from a Li-ion cell, and a schematic of various layers in the assembly. The positive electrode is typically made of a transition metal oxide, whereas the negative electrode is typically graphite. Transfer of Li ions from one electrode to another enables charging or discharging of the cell. The two electrodes are typically separated by the separator, which is typically based on an electrically insulating porous material and is about a few tens of microns thick. The separator material plays a multi-functional role [5,11].

* Corresponding author. 500 W First St., Rm 211, Arlington, TX 76019, USA. Tel.: +1 (817) 272 9338; fax: +1 (817) 272 2952.
E-mail address: jaina@uta.edu (A. Jain).

http://dx.doi.org/10.1016/j.jpowsour.2014.08.066
0378-7753/

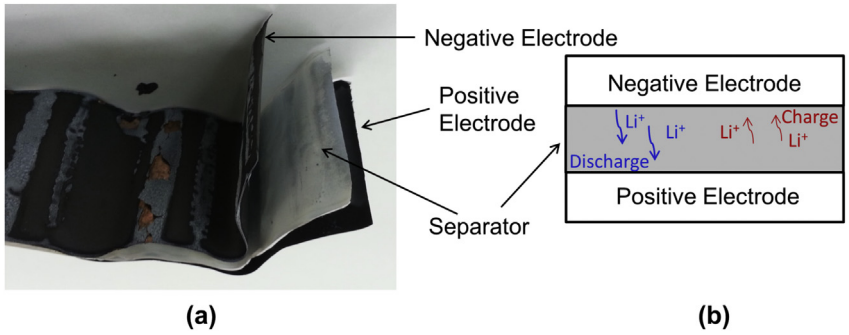

Fig. 1. (a) Image of the electrode-separator roll in a Li-ion cell; (b) Schematic of various layers in the assembly.

The primary role of the separator is to provide a pathway for Li ions to migrate from one electrode to the other while blocking electron transport [12]. The separator also provides mechanical strength without deterioration at high temperature [13,14] and contributes to conductance of heat generated inside the cell. A number of studies have been carried out for understanding and quantifying ionic conductance through the separator material [5,11]. A more limited number of studies have investigated mechanical stresses in the separator that may occur during cell operation [13–15]. Despite the importance of thermal transport within the cell, however, there is a lack of literature on measurement, modeling and optimization of thermal transport properties of the separator. Heat generated throughout the cell must conduct through the electrode roll to the outer surface, where it is eventually dissipated to the surroundings. This makes it important to understand the nature of thermal conduction with the cell [16], and rate-limiting steps that determine the effectiveness of this process [17,18]. Among all materials in the electrode roll including positive electrode ($LiFePO_4$, $LiCoO_2$, etc.), negative electrode (graphite), current collectors (metal) and separator, the separator is expected to have the lowest thermal conductivity, and hence must be investigated in detail. In addition, thermal contact resistances between the separator and electrodes may also be important. A number of papers have addressed thermal modeling within a Li-ion cell [19–22]. The accuracy of temperature fields predicted by such models depends critically on the accuracy of underlying thermal properties of constituent materials. There is a lack of experimental data on thermal properties of the separator, and most past work on thermal modeling [19–22] appears to use assumed values for thermal properties of the separator. Given the importance of accurate temperature prediction on battery safety, it is clearly very desirable to experimentally measure these properties. Such a measurement will contribute towards the thermal engineering, and hence operational safety of Li-ion cells.

The fundamental governing energy equation, the solution of which determines the temperature distribution within a thermal system is given by Ref. [23]

$$k\nabla^2 T + Q''' = \rho C_p \frac{\partial T}{\partial t} \tag{1}$$

where T is the temperature field and Q''' is volumetric heat generation rate. The two fundamental thermophysical properties that appear in this equation, and that play a key role in determining the nature of thermal transport through the separator material are its thermal conductivity, k (W m^{-1} K^{-1}) and specific heat capacity, C_p (J kg^{-1} K^{-1}) [24]. While k determines the rate of thermal conduction through the separator, C_p characterizes the extent of heat storage within the material. The quantity $k/\rho C_p$ is often referred to as the thermal diffusivity, α (m^2 s^{-1}). Note that equation (1) assumes that k is an isotropic property, although in some materials, k may be different in different directions [24].

A number of experimental techniques have been reported in the past for measurement of thermophysical properties of substrates [25–29]. In general, the temperature rise in the material of interest in response to a known heat flux is measured and compared with a theoretical model to determine k and C_p. Heat flux is imposed by either Joule heating due to an electric current, or optically through a laser. Methods based on constant, time-varying and periodic heat flux have been used in the past [25]. Two separate experiments are often required to measure both, although two measurements within the same experiment have also been used [27]. A vast amount of literature exists on the measurement of thermophysical properties of thick, rigid substrates, typically a few mm or thicker [25]. In addition, thin films, a few μm or thinner, deposited on a thick, rigid substrate have also been thermally characterized [30]. On the other hand, not much research has been reported on measurement of thermophysical properties of thin, flexible substrates. Neither of the approaches outlined above for rigid substrates or thin films will work for a substrate that is a few tens of μm, such as a typical Li-ion separator. This necessitates a new approach for thermophysical property measurement. A typical separator in a Li-ion cell is a few tens of μm thick [11,15], which presents a challenge in measurement of thermophysical properties.

An additional challenge in the measurement of thermophysical properties of a flexible substrate is in the microfabrication of heater and sensor elements. While microfabrication is carried out commonly on rigid substrates such as Silicon wafers and glass slides [31], fabrication of metal features on a thin flexible substrate is not as well developed. The mechanical stiffness of a typical separator of a Li-ion cell is even less than that of typical substrates used for flexible electronics [1,2].

This paper presents a novel experimental method for measurement of in-plane thermal conductivity and heat capacity of a Li-ion cell separator. The method is based on measurement of temperature rise in two parallel metal lines during a short time following DC heating in one of the lines. This method is capable of measurement on substrates for which experimental methods for neither thick rigid substrates, nor thin films are applicable. Measurements are in excellent agreement with an analytical model based on the assumption of a semi-infinite domain. Both in-plane thermal conductivity and heat capacity are measured at room temperature and at an elevated temperature. Results from this work are expected to contribute towards better thermal understanding and safety of Li-ion cells. Analytical modeling and experimental method are presented in next two sections, followed by a discussion of results.

2. Measurement technique

In this paper, the thermal response of a thin, flexible separator to DC heating is measured and used to determine its thermophysical properties. Since there are standard methods available for measurement of density, the two thermophysical properties of primary interest here are k and C_p. Generally, the measurement of thermal conductivity involves measurement of the steady state temperature difference sustained by a given heat flow through the material of interest. A straight-forward application of this approach is not possible for the thin and flexible separator material. It is difficult to insert standard thermocouples in this material. Similarly, application of a known heat flux is also difficult using standard experimental tools. In this paper, thin metal heaters and temperature sensors are microfabricated on the flexible substrate, and thermal response to DC Joule heating due to an electric current is measured. Fig. 2 shows a schematic of the geometry under consideration. Two parallel thin metal lines of length L are fabricated on the flexible substrate of thickness t_{subs}. The heater and sensor lines are located at $x = 0$ and $x = x_0$ respectively. The heater line bisects the flexible substrate into two halves, each of width w. The separator itself is tethered on a thick, rigid substrate at both ends ($y = \pm L/2$).

Consider the thermal effect of a DC current I_0 passing through the heater line, which has an electrical resistance of R. The heat generated in the heater line is given by:

$$Q_0 = I_0^2 R \tag{2}$$

Assuming that this experiment is carried out in vacuum, no heat loss occurs due to convection. Since the substrate is thin and free-standing, therefore no thermal conduction takes place in the out-of-plane z direction. Since the microheater line is long in the y direction, heat conduction is one-dimensional in x-direction only. Due to symmetry, half of Q_0 passes through each half of the substrate bifurcated by the heater line. The governing energy conservation equation in the separator material is given by:

$$k\frac{\partial^2 T}{\partial x^2} = \rho C_p \frac{\partial T}{\partial t} \tag{3}$$

where T is the temperature rise above ambient.

The governing equation is subject to the following boundary condition:

$$-k\left.\frac{\partial T}{\partial x}\right|_{x=0} = \frac{Q_0}{2A} = \frac{I_0^2 R}{2Lt_{subs}} \tag{4}$$

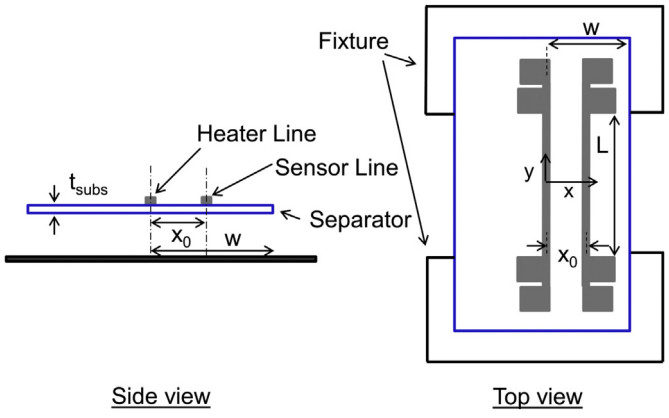

Fig. 2. Schematic of the geometry under consideration.

In addition, it may be assumed that the initial temperature is zero everywhere, i.e. $T = 0$ at $t = 0$.

A solution for the temperature distribution may be determined assuming the plastic substrate to be a semi-infinite medium for thermal conduction. This assumption is valid as long as the thermal penetration depth for the duration of the experiment, t_{exp} is much lesser than w, i.e.

$$2\sqrt{\alpha \cdot t_{exp}} \ll w \tag{5}$$

where α is the thermal diffusivity of the sample. Thus, for a given value of w, the semi-infinite assumption will be valid as long as the duration of the experiment t_{exp} satisfies

$$t_{exp} \ll \frac{w^2}{4\alpha} \tag{6}$$

Under this assumption, the solution for the transient temperature field may be derived by re-writing the energy conservation equation (Equation (3)) in terms of heat flux instead of temperature using Fourier's law. Once written in terms of heat flux, equation (3) can be easily integrated and converted back to temperature [24]. The solution for $T(x,t)$ is found to be:

$$T(x,t) = \frac{I_0^2 R}{Ak}\left[\left(\frac{\alpha t}{\pi}\right)^{\frac{1}{2}} e^{-\left(\frac{x^2}{4\alpha t}\right)} - \frac{x}{2} erfc\left(\frac{x}{\sqrt{4\alpha t}}\right)\right] \tag{7}$$

This expression forms the fundamental basis for measurement of thermal conductivity and heat capacity of the separator.

Equation (7) shows that the difference between temperature of the heater and sensor at any time is given by:

$$\begin{aligned}\Delta T(t) &= T(0,t) - T(x_0,t) \\ &= \frac{I_0^2 R}{Ak}\left[\left(\frac{\alpha t}{\pi}\right)^{\frac{1}{2}}\left(1 - e^{-\left(\frac{x^2}{4\alpha t}\right)}\right) - \frac{x}{2} erfc\left(\frac{x}{\sqrt{4\alpha t}}\right)\right]\end{aligned} \tag{8}$$

which, for large time, $t \gg x_0^2/4\alpha$, reduces to

$$\Delta T\left(t \gg \frac{x_0^2}{4\alpha}\right) = \frac{I_0^2 R x_0}{2Ak} \tag{9}$$

Thus, at large time, the difference between heater and sensor temperature becomes constant. Measurement of this temperature difference can be used in equation (9) to determine k, since all other parameters in the equation are known.

Further, in order to determine the heat capacity of the separator, the variation of the heater temperature alone with time is considered. Equation (7) shows that the temperature at the heater, $x = 0$, is given by.

$$T_{heater}(t) = T(0,t) = \frac{I_0^2 R}{Ak}\left(\frac{\alpha t}{\pi}\right)^{\frac{1}{2}} \tag{10}$$

Due to the $t^{0.5}$ term in equation (10), a log–log plot of the heater temperature as a function of time is expected to be linear, with a slope of 0.5. In addition, the intercept M of this plot is given by.

$$M = \log_{10}\left(\frac{I_0^2 R}{A\sqrt{k\rho C_p \pi}}\right) \tag{11}$$

Equation (11) shows that a measurement of the intercept of log–log plot of temperature as a function of time can be used to

determine $k \cdot C_p$, the product of thermal conductivity and volumetric heat capacity of the material, i.e.

$$kC_p = \frac{1}{\rho\pi}\left(\frac{I_0^2 R}{A10^M}\right)^2 \tag{12}$$

Once k is measured from equation (9) using temperature data from the heater and sensor, C_p can be determined from equation (13) using the heater data alone.

Note that there are two distinct requirements on the measurement time based on the requirement for the substrate to act as a semi-infinite medium, equation (6) and based on the requirement for deriving equation (9). Combining the two, it is found that the time duration for this measurement technique has upper and lower bounds given by.

$$\frac{x_0^2}{4\alpha} \ll t \ll \frac{w^2}{4\alpha} \tag{13}$$

Physically speaking, these requirements arise from the thermal wave generated from the DC current in the heater line to at least reach the sensor line, but still not reach the boundary of the separator material.

Thermal conductivity and heat capacity of the separator from a commercial 26650 Li-ion cell is measured using the technique discussed above. Microfabrication and experimental setup is described in the next section, followed by a discussion of measurement results.

3. Experiments

3.1. Microfabrication and packaging of test samples

Two Titanium metal lines are deposited in a class-100 cleanroom on a sample of separator extracted from a commercial 26650 Li-ion cell. The separator is extracted from a completely discharged 26650 Li-ion cell, and electrode materials are stripped out. Since the 26650 cell is hermetically sealed, careful attention is given to ensure safe removal of the separator. The disassembly is carried out inside a fume hood. The top of the cell is first pried off, and the casing of the cell is cut down on one side. The casing is slowly peeled back in order to provide complete access to the electrode roll. This material consists of multiple layers – separator, positive electrode, negative electrode, separator, and current collectors. Once removed, the spirally wound layers in the roll are slowly unraveled and placed flat. Layers are allowed to dry for an hour and then are manually detached from one another. The separator material is cut into samples of the desired size. Note that separator samples used in this work do not contain electrolyte, since the focus of this work is measurement of thermal properties of the separator material alone. Presence of electrolyte introduces added complications that must be addressed separately. Understanding and measuring thermal properties of the separator alone is a first step in that direction.

In order to carry out microfabrication of the metal lines on the separator material, a fixture is designed to tightly mount the separator on a rigid surface. The separator is tightly attached to a standard microscope glass slide (Fig. 3(a)) using double sided tape, and the edges are sealed by single sided tape (Fig. 3(b)). 0.3 μm Titanium is then deposited using AJA e-beam evaporator followed by photolithography using a negative mask. Metal etching is carried out in 1:1:20 mixture of HF, H_2O_2 and DI water respectively (Fig. 3(c)). Once the microheater is fabricated on the separator, the entire glass slide with separator is submerged in acetone for 10 min. This results in release of the separator from the tape (Fig. 3(d)). Each metal line is 40 μm wide and 1.8 mm long. The lines are connected to two contact pads on each end in order to facilitate four-wire measurements. The high electrical resistivity of Titanium provides the capability of large heat generation. In addition, Titanium also has a large temperature coefficient of resistivity (TCR), making it ideal for use as a temperature sensor.

The separator with microfabricated metal lines is suspended across two microscope coverslips which are mounted on microscope glass slides for ease of handling (Fig. 3(e)). Contact pads for the heater and sensor lines are then wire bonded with conductive epoxy and left to dry for 3–4 hours Fig. 3(f) shows the final microheater device with one heater line and one sensor line.

The microheater device fabricated on the separator is very flexible, and does not lose functionality even when the separator is twisted or bent. Fig. 4 demonstrates this by wrapping the separator material with metal features on the curved surface of a cylinder. Metal lines are found to be preserved and working even when the separator is significantly curved.

3.2. Calibration and thermophysical property measurements

The microheater device is calibrated in a Boeckel CCC 0.5D incubator. The device is placed inside the incubator, and the temperature is increased from 22 °C to 82 °C in steps of 15 °C. At each point, the temperature is allowed to stabilize for 15 min before measuring heater resistance. A Keithley 2612A sourcemeter is used to send a small sensing current of 10 μA, and a Keithley 2100 multimeter is used to measure the voltage difference induced across the microheater device. A plot of resistance as a function of temperature provides the required calibration for determining temperature rise during thermophysical property measurement experiments.

Experiments for thermophysical property measurement based on the technique described in section 2 are carried out in an evacuated vacuum chamber to eliminate convective heat losses. The temperature rise during each experiment is small enough to

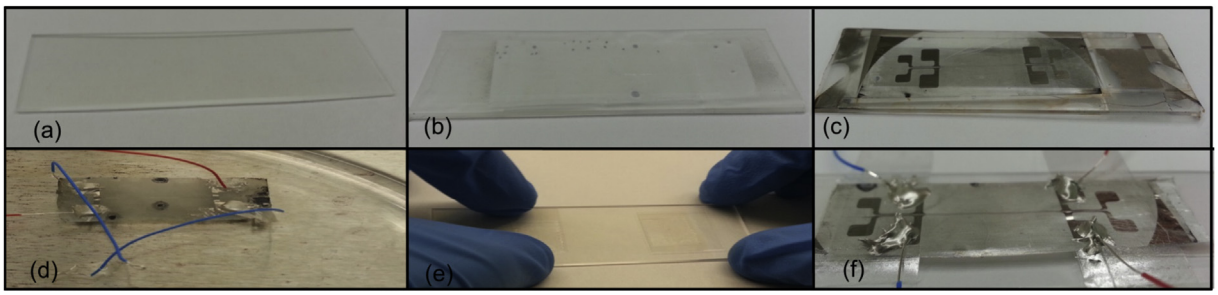

Fig. 3. Images of steps for microfabrication of microheater device. (a) Attachment to a glass slide, (b) Sealing by single sided tape, (c) Metal deposition and etching, (d) Release of the separator, (e) Attachment on a coverslip-based fixture, (f) Final device with wire bonding.

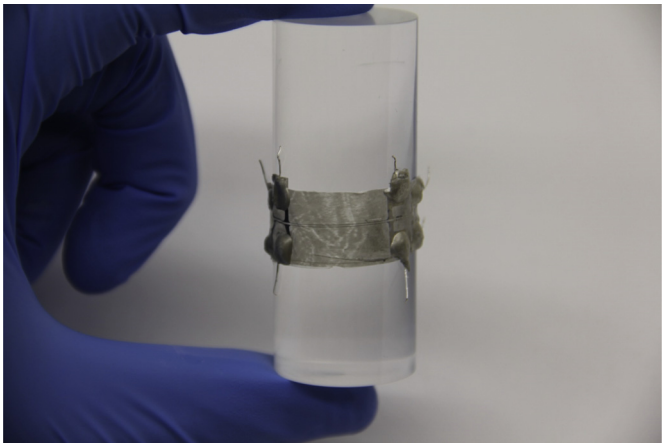

Fig. 4. Demonstration of flexibility of the device by wrapping the sample with metal features on the curved surface of a cylinder.

rule out radiation as a significant heat loss mechanism. Heating current passing through the heater line is sourced from a Keithley 2612A sourcemeter. A Keithley 2401 sourcemeter is used for sourcing a sensing current of 100 μA through the sensor for temperature measurement. This current is small enough to reliably measure the sensor resistance, and hence temperature without causing significant self-heating. A National Instruments NI-9205 cDAQ system controlled by a LabView VI is used to measure and log the heater and sensor voltages. Electrical resistance measured in this fashion is converted to temperature rise using calibration data. While the difference between the heater and sensor temperatures is used to determine k, the heater temperature alone is used to determine C_p, once k is known.

4. Results and discussion

4.1. Heater and sensor calibration, and density measurement

Measurements of heater and sensor electrical resistances as functions of temperature are shown in Fig. 5. The heater and sensor resistances are close to each other, and both exhibit a linear increase with temperature with nearly the same slope. This is expected since the heater and sensor lines are geometrically identical, and made from the same material in the same process. The measured value of thermal coefficient of resistance (TCR) for the heater and sensor is found to be 0.0022 and 0.0023 K^{-1} respectively, which are both close to the theoretically expected value of 0.0026 K^{-1} [32]. The measured slopes of these curves are used to determine heater and sensor temperatures from measured electrical resistance during experiments described in sections 4.2 and 4.3.

In order to measure the density of the separator, the thickness of a sample of known dimensions is measured by determining the step change across a sample adhered on a glass slide using a StepIQ profilometer. The sample mass is measured using a Sartorius 1712 MP balance. Using these measurements, the density of the separator is found to be 913 ± 18 kg m^{-3}.

4.2. k Measurements

Fig. 6 plots the measured temperature rise in the heater and sensor lines as a function of time for 4.6 mA heating current. The temperature difference between the two is also plotted. As expected from the theoretical model, the heater temperature initially rises faster than the sensor temperature. After some time following the start of DC heating, the difference between the two stabilizes, as expected from equation (9). It takes roughly 0.50 s for the temperature difference to stabilize, which is consistent with the lower limit predicted by equation (13).

This experiment is repeated at a number of heating currents. At each current, the temperature difference stabilizes within the expected time, and the temperature difference at this time is used to determine k from equation (9). The thermal conductivity is measured to be 0.50 ± 0.03 W m^{-1} K^{-1}. The measured room temperature thermal conductivity is close to the values assumed in previous papers on thermal analysis of Li-ion cells [19–22], although these papers are not completely clear about the source of the values used.

Note that equation (9) shows that a plot of ΔT at large time as a function of I_0^2 is expected to be linear, with a slope S_k given by:

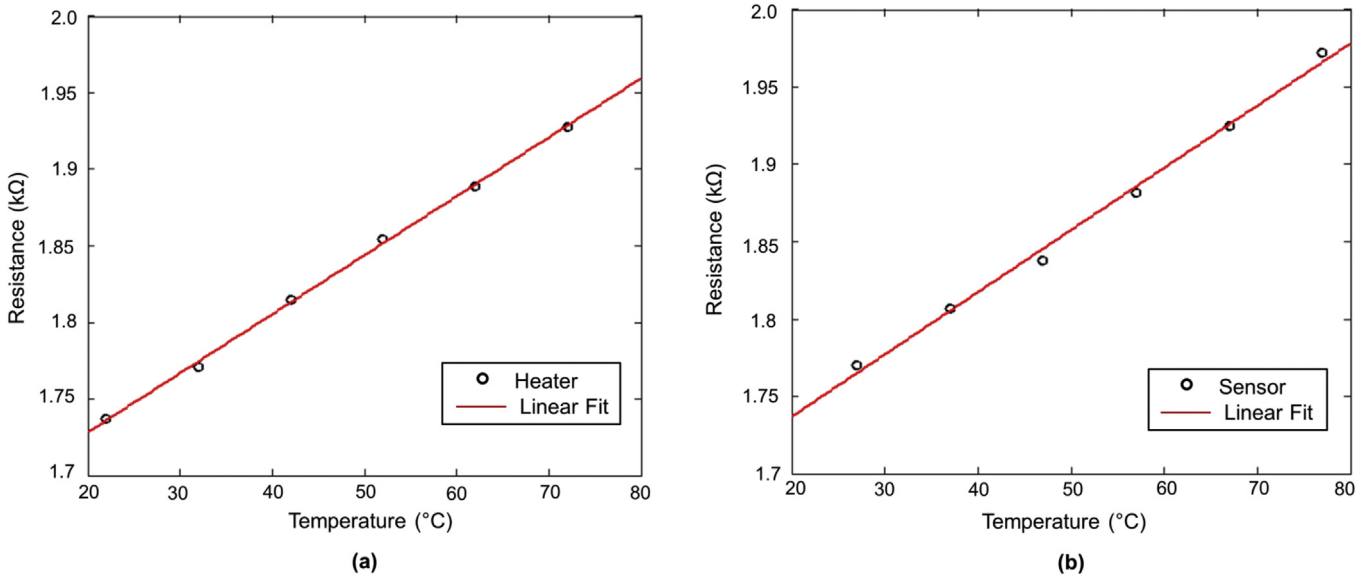

Fig. 5. Temperature calibration plots for (a) Heater line; (b) Sensor line.

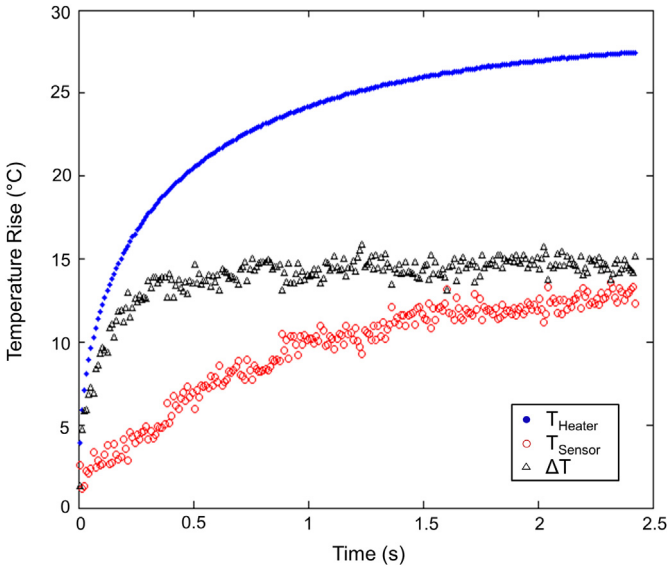

Fig. 6. Measured temperature rise in the heater and sensor lines as a function of time for 4.6 mA heating current.

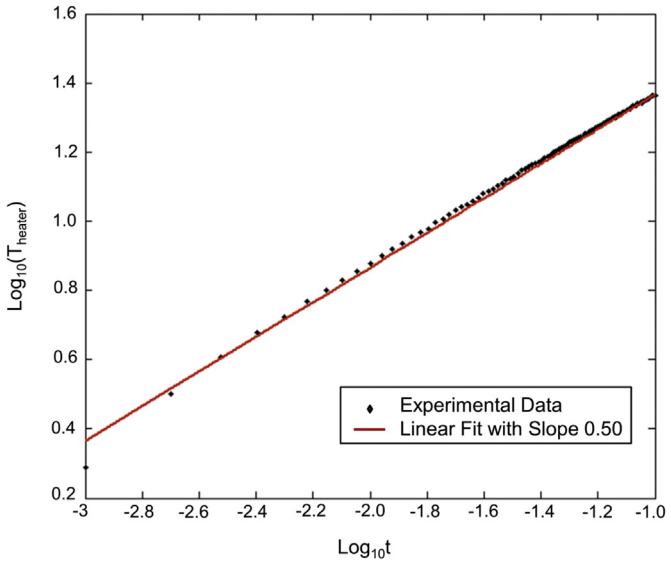

Fig. 8. Log–log plot of the measured temperature rise in the heater as a function of time for 4.6 mA.

$$S_k = \left(\frac{Rx_0}{2Ak}\right) \tag{14}$$

Fig. 7 plots the temperature difference between heater and sensor at large time as a function of the square of the heating current. As expected from equation (14), this curve is found to be linear. This shows that the experimental data is in good agreement with the analytical model presented in Section 2.

4.3. C_p measurements

Fig. 8 presents a log–log plot of the measured temperature rise in the heater for 4.6 mA heating current as a function of time up to around 2.0 s. As predicted by the analytical model, a linear fit with slope of 0.50, also shown in Fig. 8 is in good agreement with experimental data. The intercept of the data can be used to determine C_p based on equation (12). This experiment is also repeated at a number of heating currents. Fig. 9 plots the combined data. At each current, there is good agreement between experimental data and the analytical model that predicts the data to lie along a line of slope 0.50. The value of heat capacity determined from these experiments is 2480 ± 200 J kg^{-1} K^{-1}.

Equation (12) shows that a plot of 10^M as a function of I_0^2 is expected to be linear, with a slope given by:

$$S_{C_p} = \frac{R}{A\sqrt{kC_p\rho\pi}} \tag{15}$$

Fig. 10 plots 10^M as a function of I_0^2. As expected from equation (15), this curve is linear, showing that the experimental data agrees well with the analytical model for heat capacity measurement.

In order to further compare experimental data with the theoretical discussion in section 2, the heater temperature is measured for a very long time. This data, plotted on a log–log scale is

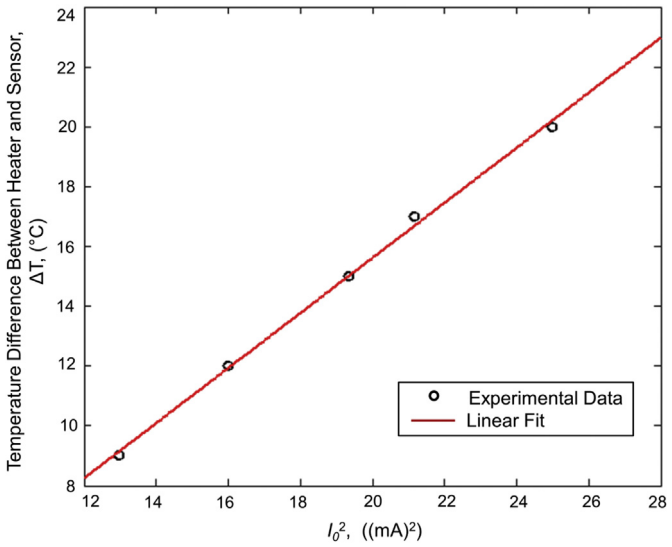

Fig. 7. Plot showing temperature difference between heater and sensor at large time as a function of the square of the heating current.

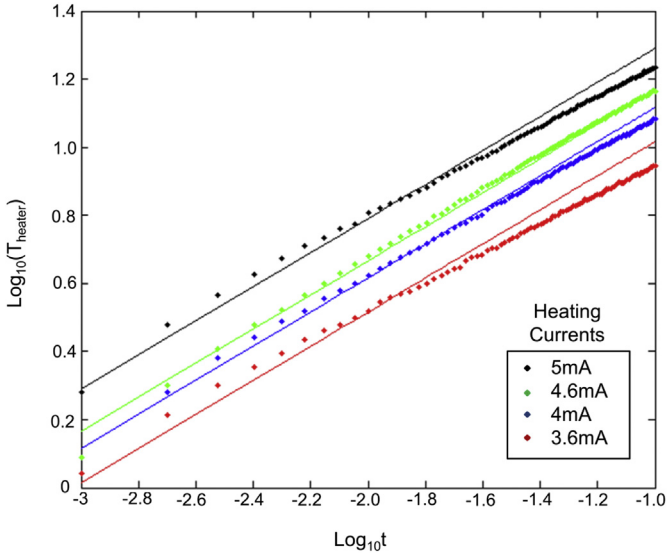

Fig. 9. Log–log plot of the measured temperature rise in the heater for multiple currents with linear fits.

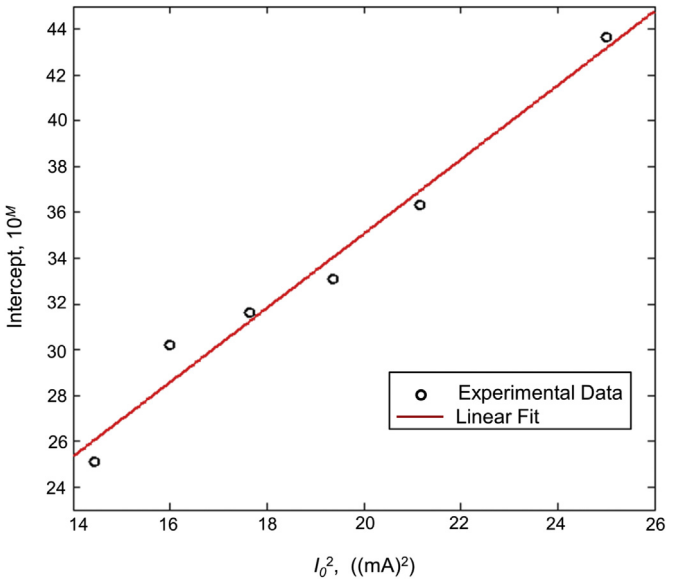

Fig. 10. Plot of intercept of log–log plots as a function of the square of the heating current.

presented in Fig. 11. It is found that for approximately the first 3.0 s, the plot fits closely with a line of slope 0.5. Beyond this time, the experimental data deviates from the 0.5 slope line, and the rate of increase in temperature is much lower than before. This is consistent with the discussion in section 2, which shows that there is an upper limit in time beyond which the semi-infinite assumption is no more valid.

Table 1 compares measured k and C_p at room temperature with values assumed by previous papers on thermal modeling [19–22]. Heat capacity values for polyethylene reported by Gaur et al. [33] are close to the present measurements, although the material used in that work is in bulk form, and may be different in morphology from the separator of a Li-ion cell. The measured thermal conductivity in this paper is slightly higher than the recently measured overall cell-level radial thermal conductivity

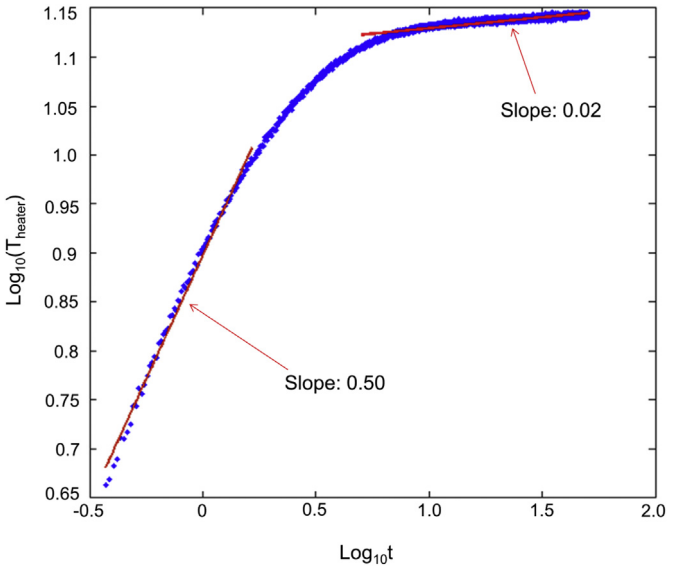

Fig. 11. Log–log plot of the measured temperature rise in the heater for a large time duration.

Table 1
Comparison of measured k and C_p at room temperature with values assumed by previous papers on thermal modeling.

	Chen et al. [21]	Wu et al. [20]	Peyman & Bahrami [19]	Kim et al. [22]	Current work
k (W m^{-1} K^{-1})	0.3344	1.29	0.34	1.0	0.5 ± 0.03
C_p (J kg^{-1} K^{-1})	1978	1839	1987	700	2480 ± 300
ρ (kg m^{-3})	1008.98	1043	1017	1200	913 ± 18

[16], which indicates the additional impedance to heat flow may be occurring due to thermal contact resistance at interfaces between various materials in the electrode-separator stack.

4.4. k and C_p measurements at high temperature

Thermal performance of the separator is particularly important at high temperature. Ineffective heat dissipation during high temperature operation may result in heat buildup and temperature rise, which may eventually lead to a thermal runaway situation. As a result, it is important to understand and measure thermal properties of the separator at high temperature. The experiments described in previous sections are repeated in a 50 °C ambient with all other experimental conditions being the same as previous experiments. Table 2 summarizes the room temperature (25 °C) and high temperature (50 °C) measurements of thermal conductivity and heat capacity. It is found that there is negligible change in both thermal conductivity and heat capacity between 25 °C and 50 °C. The small change in the properties between these temperatures is within the measurement error. As a result, thermal conductivity and heat capacity of separator material in a Li-ion cell may be assumed to be independent of temperature in the range of interest for modeling and simulation of thermal performance and safety of Li-ion cells.

4.5. Experimental error analysis

The main sources of experimental error in the measurement of k and C_p arise from measurement of the cross-section area A of the separator. Other errors, including instrument least count errors, etc. are negligible. Based on a relative error analysis, the experimental errors in thermal conductivity and heat capacity measurements are estimated to be 6% and 12% respectively. The error in heat capacity measurement is greater, since heat capacity is determined based on the measurement of k, and thus, relative error in measuring k also contributes towards relative error in C_p, in addition to other sources of error.

5. Conclusions

The separator material is expected to have the lowest thermal conductivity among all materials in the electrode stack of a Li-ion cell. This paper presents a novel experimental method to measure the in-plane thermal conductivity and heat capacity of the

Table 2
Measured thermal conductivity and heat capacity of Li-ion cell separator at room temperature and at elevated temperature.

	k (Wm^{-1} K^{-1})	C_p (J kg^{-1} K^{-1})
Room Temperature (25 °C)	0.50 ± 0.03	2480 ± 300
Elevated Temperature (50 °C)	0.43 ± 0.03	2470 ± 300

separator from a Li-ion cell. Experimental data from this measurement method, based on a thermally semi-infinite domain in the separator, are found to be in excellent agreement with the underlying theoretical model. Data suggest that the separator has poor thermal conductivity, which does not change significantly at higher temperature. Measurements presented in this paper contribute towards the understanding of thermal conduction within a Li-ion cell, and provide useful thermal property data that has so far been missing from the literature for a material of much importance for ensuring safety and performance of Li-ion cells.

Acknowledgments

Microfabrication described in this paper was carried out at the Nanotechnology Research and Education Center at the University of Texas, Arlington.

References

[1] Y. Sun, J.A. Rogers, Adv. Mater. 19 (2007) 1897–1916.
[2] W.S. Wong, A. Salleo, Flexible Electronics: Materials and Applications, first ed., Springer, 2009.
[3] M. Armand, J.-M. Tarascon, Nature 451 (2008) 652–657.
[4] B. Scrosati, J. Garche, J. Power Sources 9 (2010) 2419–2430.
[5] V. Etacheri, R. Marom, R. Elazari, G. Salitra, D. Aurbach, Energy Environ. Sci. 4 (2011) 3243–3262.
[6] S.R. Forrest, Nature 428 (2004) 911–918.
[7] W.A. MacDonald, M.K. Looney, D. MacKerron, R. Eveson, R. Adam, K. Hashimoto, K. Rakos, J. Soc. Inf. Displ 15 (2012) 1075–1083.
[8] J.A. Rogers, Z. Bao, K. Baldwin, A. Dodabalapur, B. Crone, V.R. Raju, V. Kuck, H. Katz, K. Amundson, J. Ewing, P. Drzaic, Proc. Nat. Acad. Sci. U S A 98 (2001) 4835–4840.
[9] Y. Chen, J. Au, P. Kazlas, A. Ritenour, H. Gates, M. McCreary, Nature 423 (2003) 136.
[10] X.M. Tao, Wearable Electronics and Photonics, Elsevier, 2005.
[11] S.S. Zhang, J. Power Sources 164 (2007) 351–364.
[12] S.J. Harris, A. Timmons, D.R. Baker, C. Monroe, Chem. Phys. Lett. 485 (2010) 265–274.
[13] X. Xiao, W. Wu, X. Huang, J. Power Sources 195 (2010) 7649–7660.
[14] J. Christensen, J. Electrochem. Soc. 157 (2010) A366–A380.
[15] G. Venugopal, J. Moore, J. Howard, S. Pendalwar, J. Power Sources 77 (1999) 34–41.
[16] S.J. Drake, D.A. Wetz, J.K. Ostanek, S.P. Miller, J.M. Heinzel, A. Jain, J. Power Sources 252 (2014) 298–304.
[17] K. Shah, S.J. Drake, D.A. Wetz, J.K. Ostanek, S.P. Miller, J.M. Heinzel, A. Jain, J. Power Sources 258 (2014) 374–381.
[18] K. Shah, S.J. Drake, D.A. Wetz, J.K. Ostanek, S.P. Miller, J.M. Heinzel, A. Jain, J. Power Sources 271 (2014) 262–268.
[19] T. Peyman, M. Bahrami, SAE Int. J. Passeng. Cars Electron. Electr. Syst. 5 (2012) 164–176.
[20] W. Wu, X. Xiao, X. Huang, in: ASME 2011 5th International Conference on Energy Sustainability, 2011, pp. 1513–1522.
[21] S.C. Chen, C.C. Wan, Y.Y. Wang, J. Power Sources 140 (2005) 111–124.
[22] U.S. Kim, C.B. Shin, C. Kim, J. Power Sources 189 (2009) 841–846.
[23] F.P. Incropera, D.P. Dewitt, Introduction to Heat Transfer, third. ed., Wiley Inc, 2006.
[24] N. Ozisik, Heat Conduction, second ed., John Wiley & Sons, 1993.
[25] D.G. Cahill, K.E. Goodson, A. Majumdar, Trans. ASME J. Heat Transf. 124 (2002) 223–241.
[26] L. Shi, D. Li, C. Yu, W. Jang, D. Kim, Z. Yao, P. Kim, A. Majumdar, Trans. ASME J. Heat Transf. 125 (2003) 881–888.
[27] A. Jain, K.E. Goodson, ASME J. Heat Transf. 130 (2008) 1–7.
[28] D. Cahill, Rev. Sci. Instrum. 61 (1990) 802–808.
[29] K. Kurabayashi, M. Asheghi, M.N. Touzelbaev, K.E. Goodson, IEEE/ASME J. MicroElectroMechanical Syst. 8 (1999) 180–191.
[30] D.G. Cahill, M. Katiyar, J.R. Abelson, Phys. Rev. B 50 (1994) 6077–6081.
[31] G.T.A. Kovacs, Micromachined Transducers Sourcebook, second ed., McGraw-Hill, New York, 1984.
[32] M.J. Donachie, Titanium: a Technical Guide, second ed., ASM International, 2000.
[33] U. Gaur, B. Wunderlich, J. Phys. Chem. Ref. Data 10 (1981) 119–152.